PALAGONITIC (NOT ANDESITIC) MARS: EVIDENCE FROM THERMAL EMISSION AND VNIR SPECTRA OF PALAGONITIC ALTERATION RINDS ON BASALTIC ROCK. R. V. Morris[1], T. G. Graff[2], S. A. Mertzman[3], M. D. Lane[4], P. R. Christensen[2], [1]NASA Johnson Space Center, Houston, TX 77058 (richard.v.morris@nasa.gov), [2]Dept. of Geol. Sci., Arizona State University, Tempe, AZ 85287, [3]Dept. of Geosci., Franklin and Marshall College, Lancaster, PA 17604, [4]Planetary Science Institute, Tucson, AZ 85705.

Introduction: Visible and near-IR (VNIR) spectra of both Martian bright and dark regions [e.g., 1-6] are characterized by a ferric absorption edge extending from ~400 to 750 nm, with bright regions having about twice the reflectivity at 750 nm as dark regions. Between 750 nm to beyond 2000 nm, bright and dark regions have nearly constant and slightly negative spectral slopes, respectively. Depending on location, bright regions have shallow reflectivity minima in the range 850-910 nm that are attributed to ferric oxides. Similarly, dark regions have shallow reflectivity minima near ~950 and 1700-2000 nm that are attributed to ferrous silicate minerals (pyroxene).

Among terrestrial geologic materials, the best spectral analogues for Martian bright regions are certain palagonitic tephras from Mauna Kea Volcano (Hawaii) [e.g., 7-12]. By definition [13], palagonite is "a yellow or orange isotropic mineraloid formed by hydration and devitrification of basaltic glass." The ferric pigment in palagonite is nanometer-sized ferric oxide particles (np-Ox) dispersed throughout the hydrated basaltic glass matrix [10-12]. The hydration state of the np-Ox particles is not known, but the best Martian spectral analogues contain allophane-like materials and not crystalline phyllosilicates [12].

Mars Global Surveyor thermal emission spectra (TES) show mid-IR evidence for andesitic and basaltic volcanic compositions preferentially found in northern (Acidalia) and southern (Syrtis Major) hemispheres, respectively [e.g., 14-16]. The absence of a ferric-bearing component in the modeling of TES spectra is in apparent conflict with VNIR spectra of Martian dark regions, as discussed above. However, [17] have interpreted the andesitic spectra as oxidized basalt using phyllosilicates instead of high-SiO_2 glass as endmembers in the spectral deconvolution.

We show here that laboratory VNIR and TES spectra of palagonitic alteration rinds developed on basaltic rocks are spectral endmembers that provide a consistent explanation for both VNIR and TES data of Martian dark regions.

Samples and Methods: Most of our work was done on basaltic rock HWMK124, which was collected at an elevation of ~4000 m on Mauna Kea Volcano (Hawaii). The rock had a brown rind over the entire exterior surface. During collection, an internal fracture surface was exposed, and it had a white rind. The rock was sawed to slabs ~1 cm thick, with opposing rind and saw surfaces. Rinds were ~100 μm thick, based on binocular examination of polished saw cuts normal to the rind. Several slabs of unaltered rock with opposing polished surfaces (60 and 600 grit polish) were made to produce additional surface textures. Two size fractions of unaltered rock were also prepared. The 500-1000 μm size fraction was obtained by mechanical grinding and wet (ethanol) sieving. The <5 μm size fraction was prepared by pulverization of unaltered rock in a ball mill followed by ultrasonic dispersement and sedimentation (both in H_2O at pH = 9) using a density of 2.65 g/cm^3 to calculate settling times [18].

For purposes of comparison, we also obtained TES spectra for the 500-1000 μm size fractions of basaltic glass (Kilauea Volcano, HI), opal-C/T (Providence Mountains, NV), obsidian (Mineral Co., NV), and an allophane-like material (Magdalena, NM).

Thermal emission spectra (5-50 μm) were obtained using a modified Nicolet Nexus E.S.P. FT-IR spectrometer [19]. VNIR spectra (0.35-2.1 μm) were obtained using a Cary-14 diffuse reflectance spectrometer [11]. Both emissivity and VNIR spectra were obtained under desiccating conditions (N_2 purge gas derived from liquid N_2). XRD and XRF data were obtained on fine powders of all samples using methods described in [e.g., 11].

Results: Major element concentrations are compiled in Table 1. HWMK124 and HWKV201 are basaltic in bulk composition. The elemental composition for the <5 μm size fraction of HWMK124 is significantly different from its parent basalt, presumably from contamination by the alumina components of the ball mill or from differential comminution of the basalt or both. From the XRD powder diffraction patterns, the major crystalline phases are plagioclase feldspar, olivine, pyroxene, and ilmenite. The samples of obsidian, opal-C/T, and allophane are high in SiO_2 + Al_2O_3. The basalt and obsidian samples are volatile poor (LOI <1%), and the opal-C/T and allophane samples are volatile rich (LOI = 8 – 28%).

Table 1. Major element concentrations and loss on ignition (LOI) in wt.%.

	1	2	3	4	5	6
SiO_2	48.30	50.81	49.82	93.41	75.64	14.06
TiO_2	3.27	1.76	2.33	0.05	0.10	0.00
Al_2O_3	13.45	19.55	13.10	1.44	13.17	78.46
Fe_2O_3T	14.72	8.82	12.66	0.52	0.79	0.13
MgO	5.86	3.89	7.69	3.35	0.08	0.13
CaO	10.70	9.89	10.63	0.23	0.57	0.62
Na_2O	2.69	3.57	2.21	0.26	4.33	3.34
K_2O	0.75	0.95	0.40	0.32	4.80	0.01
P_2O_5	0.40	0.49	0.23	0.02	0.01	0.03
Total	100.46	98.87	99.38	99.64	99.75	99.44
LOI	0.76	0.93	0.44	8.15	0.14	27.81
FeO	11.62	6.91	10.14	0.19	0.40	0.12
Fe_2O_3	1.81	1.14	1.38	0.31	0.35	0.00

1 = HWMK124 unaltered interior, 2 = HWMK124 <5 μm, 3 = HWKV201 (basaltic glass), 4 = PMDCDY1 (opal-C/T), 5 = GLMPNV5 (obsidian), 6 = JMNM1 ("allophane").

TES and VNIR spectra for samples derived from the interior of HWMK124 (unaltered basalt) are shown in Figure 1. The expected decrease in TES spectral contrast (without change in position) for the reststrahlen bands with increasing surface roughness [e.g., 20] from the most polished surface (600 grit) to the 500-1000 μm size fraction is observed. For the <5 μm size fraction and in agreement with behavior at very small particle size [e.g., 20], the reststrahlen bands are absent, with only the Christiansen (~1280 cm^{-1}) and transparency (845 cm^{-1}) features present. All VNIR spectra show a shallow band minimum near 1020 nm which is consistent with ferrous iron in the olivine observed in XRD data. For slabs, there appears to be an increasingly more negative spectral slope with increasing surface roughness.

The TES and VNIR spectra for the brown rinds on the rock are shown in Figure 2. The TES spectra display a range in behavior. Spectra at two locations (rind B and C) are nearly equivalent to that for the 500-1000 μm size fraction of unaltered rock. At three other locations (rind E1, E2, and D), the reststrahlen bands for the underlying rock are completely masked by the reststrahlen bands for the rind itself. This difference in behavior is not understood, but it may be related to rind thickness and how well the rind is coupled to the underlying rock substrate. The general shape of the brown rind spectrum (reststrahlen bands near 1100 and 450 cm^{-1}) is similar to that for other amorphous or poorly-crystalline materials (allophane, basaltic glass, and opal-C/T in Figure 3) but not similar to those for phyllosilicates (Figure 4) that have an additional band near 530 cm^{-1}. The VNIR spectra for the brown rinds are all similar and are characterized by a Fe^{3+} absorption edge. Note that in all cases the rind did not mask the Fe^{2+} feature associated with olivine (Figure 3c)

The TES and VNIR spectra of the brown rinds, together with the results of previous studies of palagonitic tephra [10-12] and exposed surfaces of young (<1.5 ka) Mauna Loa and Kilauea basaltic rocks [e.g., 21-23], imply a palagonitic rind on HWMK124. That is, basaltic glass exposed on the surface underwent hydration which, under oxidizing conditions, resulted in precipitation of nanometer sized ferric oxide particles in an amorphous, hydrated glass (allophane-like) matrix that is enriched in SiO_2 + Al_2O_3 relative to the initial basaltic glass. The oxide particles are the pigment responsible for the Fe^{3+} absorption edge in VNIR spectra and the allophane-like matrix is the origin of the 1093 and 463 cm^{-1} bands in TES spectra. The feature at 1093 cm-1 is the "B" spectral feature described by [21-23].

The TES and VNIR spectra for the white rind found in an interior fracture surface of HWMK124 are shown in Figure 3. We believe this rind is opaline silica based on its similarity to the TES spectrum of opal-C/T and the absence of a Fe^{3+} absorption edge (Figure 3c). The TES spectrum is also very similar to the thickest opaline silica coating deposited on a basaltic substrate in laboratory experiments [24]. We suggest that silica was aqueously leached from the parent rock and deposited in the fracture as an accretionary deposit of opaline silica.

Applications to Mars:

Palagonitic versus Andesitic Mars. In Figure 4 we compare TES spectra for palagonitic rind D, two phyllosilicates (Fe-smectite and Ca-montmorillonite), and high-SiO_2 glass (obsidian). The TES spectra for the phyllosilicates were obtained from the Arizona State University spectral library (version 1.5). The phyllosilicates and high-SiO_2 glass were used as endmembers to model the Acidalia-type surface with the result that [14-16] concluded that andesitic material is present and [17] concluded weathered basalt is present. These seemingly contradictory results are possible because the spectral region where the phyllosilicates and high-SiO_2 glass can be distinguished (~532 cm^{-1}) is excluded for surface modeling by atmospheric CO_2 [e.g., 14]. Because the palagonitic rind spectrum is similar to the high-SiO_2 glass spectrum at all wavenumbers and to the phyllosilicate spectra except in the ~532 cm^{-1} excluded region, it follows that Acidalia surface can be modeled with palagonitic alteration rinds on basaltic rocks.

Although this study and [17] come to the same general conclusion regarding the possible nature of the Acidalia surface based on TES spectra (i.e., weathered basalt), we suggest that palagonitic material is favored over phyllosilicates on the basis of the absence of strong phyllosilicate H_2O/OH features near 1400 and 1900 nm [e.g., 5, 6] and the presence of a ferric absorption edge in Martian VNIR spectra. We favor palagonitic Mars, but cannot exclude andesitic Mars, based on the similarity of the VNIR spectra for Acidalia and Syrtis surface regions [4].

Composition of Martian Dust. Figure 5a shows that the TES spectrum for the <5 μm size fraction of HWMK124 is virtually identical to the corresponding spectrum for Martian high albedo surfaces [25] over the region 200-1350 cm^{-1}, implying an unaltered basaltic component in the dust. However, the HWMK124 dust does not have a ferric absorption edge (Figure 1) that is a characteristic of Martian bright regions. The TES and VNIR constraints suggest Martian dust is a mixture of unaltered or weakly altered basalt and palagonitic material, including a contribution from palagonitic rock rinds [26].

Basaltic Surface Endmembers for Mars. The presence of ferric absorption edges for both Syrtis and Acidalia surfaces [4] implies that both might be mixtures to different degrees of basalt and weathered basalt. In Figure 5b we show the Syrtis and Acidalia spectra as published by [14] and two endmember spectra calculated assuming linear mixing and Syrtis and Acidalia surfaces that are 30% and 60% unaltered basalt, respectively. The calculated endmembers, corresponding to weathered basalt and unaltered basalt, are spectra calculated for 0% and 100% unaltered basalt, respectively. The weathered basalt endmember may imply that a distribution of palagonite-like spectra are present in which positional distribution of the ~1000 cm^{-1} feature is larger than that for the ~460 cm^{-1} feature. This is supposition not unreasonable on the basis of the spectra shown in Figure 3. Qualitatively, the shape of the calculated basalt endmember implies higher proportions of olivine.

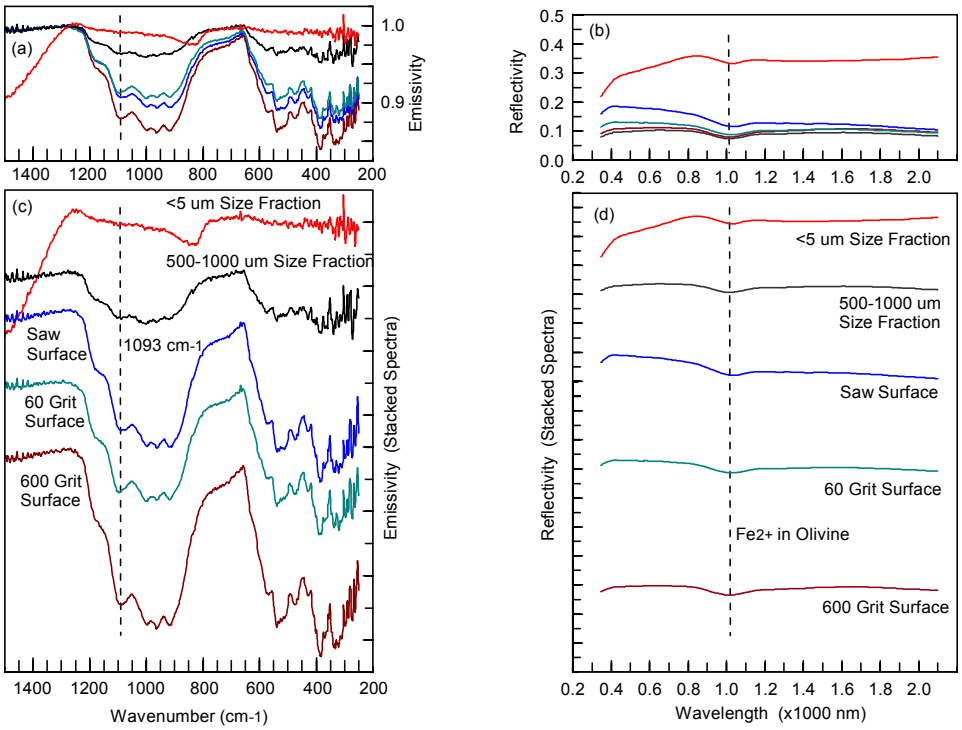

Figure 1. TES (a and c) and VNIR (b and d) spectra for unaltered basaltic rock HWMK124. Spectra are from size fractions of interior rock and slabs of unpolished and polished (60 and 600 grit) sawed surfaces.

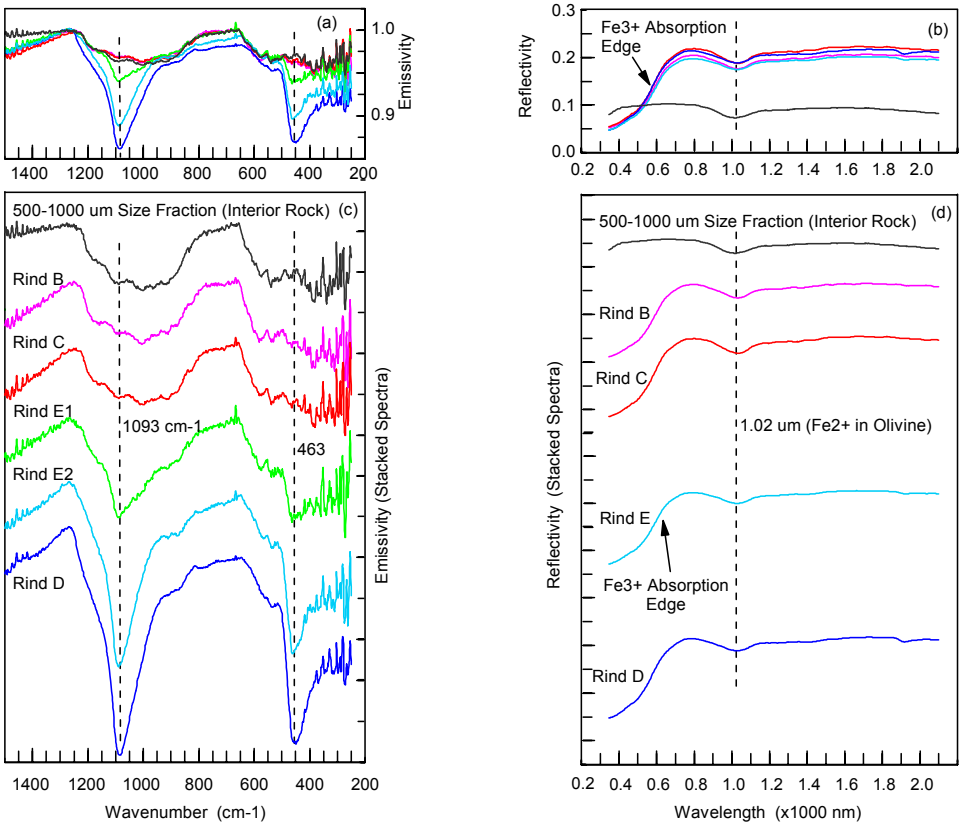

Figure 2. Thermal emission (a and c) and VNIR spectra (b and d) for basaltic rock HWMK124. Spectra are derived from brown (palagonitic) rinds on exterior surfaces and from the 500-1000 um size fraction of ground and sieved interior (unaltered) rock.

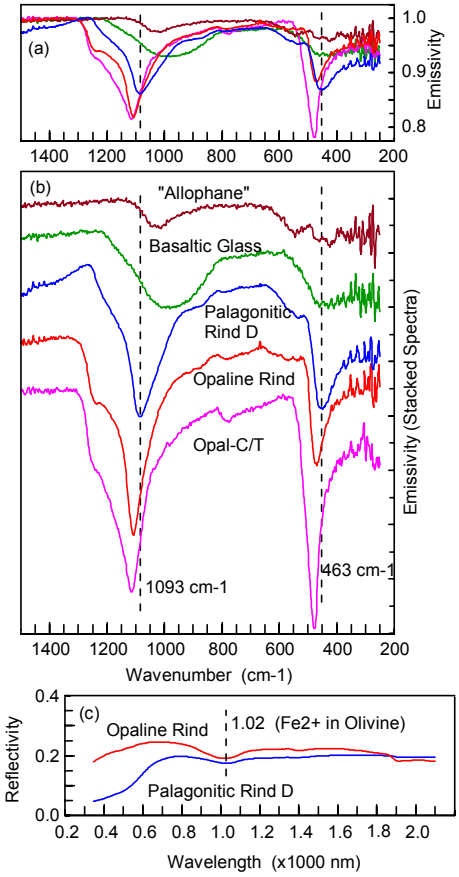

Figure 3. TES (a and b) and VNIR (c) spectra for amorphous or poorly crystalline materials.

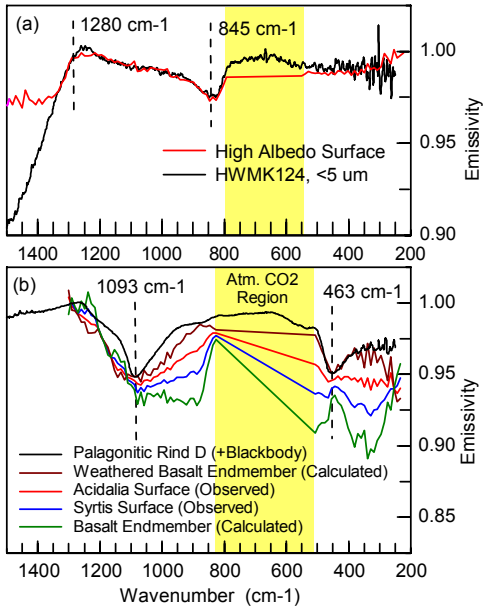

Figure 5. TES spectra (a) for Martian high albedo surface and the <5 μm size fraction of HWMK124 and (b) for palagonitic rind, Acidalia and Syrtis surfaces, and calculated basaltic endmembers.

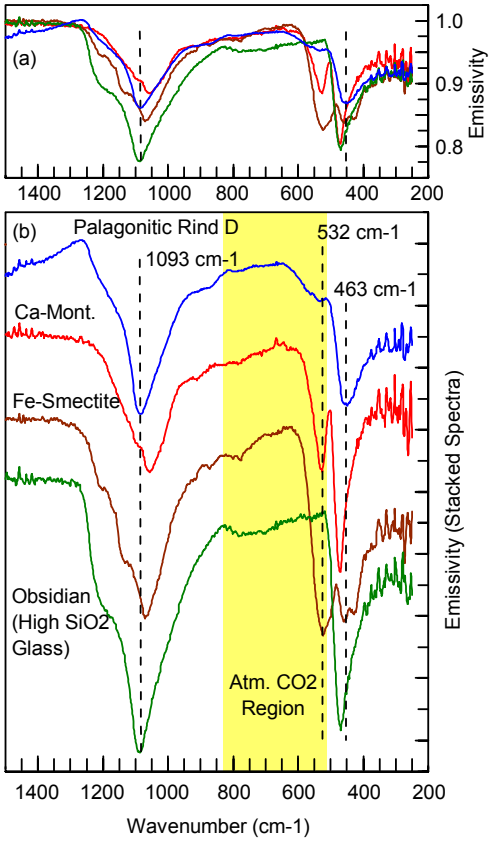

Figure 4. Comparison of TES spectra (a and b) for palagonitic rinds, two phyllosilicates, and high-SiO_2 glass (obsidian).

References: [1] Singer et al. (1979) *JGR, 84*, 8415. [2] Mustard and Bell (1994) *GRL, 21*, 353. [3] Erard and Calvin (1997) *Icarus, 130,* 449. [4] Morris et al. (2002) *LPS 33*, #1913. [5] Mustard et al. (1997), *JGR, 102*, 25605. [6] Murchie et al. (1993) *Icarus*, *105*, 454-468. [7] Evans and Adams (1979) *PLPSC, 10,* 1829. [8] Singer (1982) *JGR, 87*, 10159. [9] Morris et al. (1990) *JGR, 95*, 14427. [10] Morris et al. (1993) *GCA, 57*, 4597. [11] Morris et al. (2000) *JGR, 105*, 1757. [12] Morris et al. (2001) *JGR, 106*, 5057. [13] Bates and Jackson (1984) *Dict. Geol. Terms*, Doubleday, NY. [14] Bandfield et al. (2000) *Science, 287,* 1626. [15] Christensen *et al*. (2001) *JGR, 106,* 23823. [16] Hamilton et al. (2001) *JGR, 106*, 14733. [17] Wyatt and McSween (2002) *Nature, 417*, 263. [18] Jackson, M. L. (1985) *Soil Chemical Analysis--Advanced Course*, 895 pp., Madison, Wis. [19] Ruff S. W. et al. (1997) *JGR, 102*, 14899. [20] Salisbury (1993), *Remote Geochem. Anal.*, Cambridge, 79. [21] Kahle et al. (1988) *JGR, 93*, 15,239. [22] Kahle et al. (1995) *Mauna Loa Revealed*, Geophys. Monograph 92, 145. [23] Crisp and Bartholomew (1992) *JGR, 97*, 14,691. [24] Kraft et al. (2003) *LPS 34*, #1420. [25] Bandfield and Smith (2003) *Icarus*, 161. [26] Morris et al. (2003), *LPS 34*, #1874.